Journal of Physics Communications

PAPER

Comparison of optical trapping wavelengths for nanoscopic diamonds containing nitrogen-vacancy centers

Srestha Roy[1,4], **Atanu Ghosh**[2,3,4], **Muruga Lokesh**[1], **Gokul Nalupurackal**[1], **Snigdhadev Chakraborty**[1], **Jayesh Goswami**[1], **Vidya P Bhallamudi**[1], **Siddharth Dhomkar**[2,3,*] and **Basudev Roy**[1,*]

[1] Department of Physics, Quantum Centres in Diamond and Emergent Materials (QuCenDiEM)-group, Indian Institute of Technology Madras, Chennai, 600036, India
[2] Department of Physics, Indian Institute of Technology Madras, Chennai, 600036, India
[3] Center For Quantum Information, Communication And Computing (CQuICC), Indian Institute of Technology Madras, Chennai, 600036, India
[4] These authors are contributed equally to this work.
[*] Authors to whom any correspondence should be addressed.

E-mail: sdhomkar@physics.iitm.ac.in **and** basudev@iitm.ac.in

Keywords: diamonds with NV centers, optical tweezers, NV photoluminescence

OPEN ACCESS

RECEIVED
17 January 2024

REVISED
17 April 2024

ACCEPTED FOR PUBLICATION
8 May 2024

PUBLISHED
16 May 2024

Abstract

In this article, we explore the effect of two different infrared (IR) laser wavelengths on the optical properties of trapped nano-diamonds containing high-density ensembles of nitrogen vacancy (NV) centers. We investigate 975 nm and 1064nm wavelengths for trapping lasers and find that NV photoluminescence quenching is more prominent for 1064nm illumination than for 975 nm illumination when simultaneously excited with a 532 nm laser. In order to understand the underlying mechanism, we develop a rate-equation-based model that takes into account various transition probabilities. The model suggests that the findings cannot be explained only by imposing modification of the NV charge-state ratio under varied illumination wavelengths, and, thus, we speculate that the effective ionization and recombination rates associated with NV charge states for the studied samples are highly wavelength-dependent in the probed regime. Importantly, the results demonstrate that 975 nm laser is desirable for optical trapping of NV-diamonds, especially for NV-based sensing applications.

1. Introduction

Nitrogen-vacancy (NV) center, an optically active spin defect in diamond, is an excellent candidate for room temperature quantum sensing [1–4] due to its unique properties, such as all-optical spin initialization and spin readout, relatively long coherence lifetime, high quantum yield, etc [5]. The strength of NVs originates from their unique level structure. When NVs are excited with a 532nm green laser, the photoluminescence (PL) spectrum displays two zero phonon lines (ZPLs) at 637 nm and 575 nm corresponding to negatively charged (NV^-) and neutral charge state (NV^0) and a large phonon side-band extending up to 800 nm wavelength [5, 6]. Amongst the two charge states, NV^- is a spin-1 system with a triplet ground state, which can be readily initialized and readout via an optical excitation, typically with green light at ~532 nm, owing to the inter-system crossing mechanism [5]. The spin states of NV^- can be controlled by applying appropriate static and radio-frequency magnetic fields, transforming this defect into a versatile nanoscopic sensor [7–11]. Interaction of NV centers with localised surface plasmons in metals results in interesting changes in emission properties [12, 13]. Additionally, nano/micro-diamonds containing NV centers are fully biocompatible [14, 15] with immense functionalization possibilities [16]. Thus, NVs residing in nano/micro-diamonds can be utilized for diverse biosensing applications from bio-marking to magnetometry [17–22]. Furthermore, the ability to trap NV nanodiamonds using optical tweezers provides an additional knob for controlling position and motion of this sensor [23–26]. Optical trapping is mostly achieved using IR laser beams as the absorption by biological samples is minimal in this region. However, the presence of IR trapping laser has been consistently shown to significantly

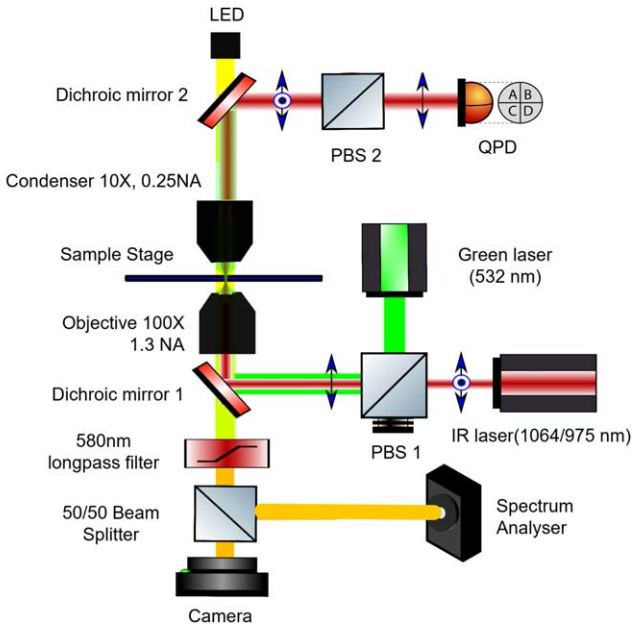

Figure 1. Schematic of the experimental setup to measure the photoluminescence spectra of trapped nanodiamonds.

lower the NV PL intensity [23, 27–30]. The sensitivity of NVs is inherently tied to the PL efficiency, and thus finding a reliable trapping laser is essential for performing sensing experiments.

Although NV PL quenching under IR illumination is a well-reported phenomenon [30, 31], there is no consensus on the underlying mechanism. The quenching is generally attributed to complex charge dynamics in diamonds [28–30, 32], however, a systematic study comparing the effects of varied IR illumination wavelengths is unavailable. In this manuscript, we show that two trapping lasers with wavelengths 975 nm and 1064nm have identical trapping characteristics, but have a visibly distinct influence on the optical properties of NVs. Specifically, the results demonstrate that in conjunction with green laser for excitation, a 975 nm laser is well suited for trapping NV nanodiamonds due to two to three times less PL quenching in the relevant power density regime. Furthermore, by means of simulation, we show that in the infrared regime, the ionization and recombination rates for the two prominent charge states of the NV center are highly wavelength dependent. Specifically, the rates are significantly higher for an illumination wavelength of 1064nm than those for an illumination wavelength of 975 nm, in the presence of a green (532 nm) laser, used as a primary source excitation.

2. Experimental details

Nanodiamonds (≈diameter 0.5 μm, MDNV1umHi10mg, [26] 3ppm NV centers, Adamas Nanotechnologies) were trapped with optical tweezers using an infrared laser. The optical trap is set up using the optical Tweezer kit (OTKB, Thorlabs), shown in figure 1. The infrared lasers used for trapping the nanoparticles are passed through a polarizing beam splitter (PBS). These polarized beams are made to fall onto a dichroic mirror which reflects the beam towards an objective lens (1.3 NA, 100×, Olympus, oil immersion). The objective tightly focuses the beam onto the sample stage.

On the sample stage, a suspension of the microparticles in water is placed between a glass coverslip and a glass slide. The incident light is partially scattered by the particles in the sample chamber and the forward propagating beam containing scattered and unscattered light is collected by a condenser(10 ×, 0.25 NA, Nikon) which passes the beam to another IR reflecting dichroic mirror. The subsequent reflected beam is then split into two orthogonal polarization components by another polarizing beam splitter. The transmitted beam is passed onto a quadrant photodiode for position detection. To excite the trapped nanodiamonds, a 532 nm green laser (diode pumped solid state laser) is passed along with the IR through the orthogonal face of the polarising beam splitter which reflects the polarised green light into the sample chamber similar to the IR beam. The dichroic mirror partially allows the green light. A CMOS camera in the back focal plane is used for imaging. A visible LED source is used to illuminate the sample chamber. The nanodiamonds absorb green light and emit red. Therefore, a 580 nm long-pass filter in the back focal plane is used to filter out all visible wavelengths other than red. This filtered backscattered light is split by a 50:50 beam splitter. One component is sent to the camera for imaging,

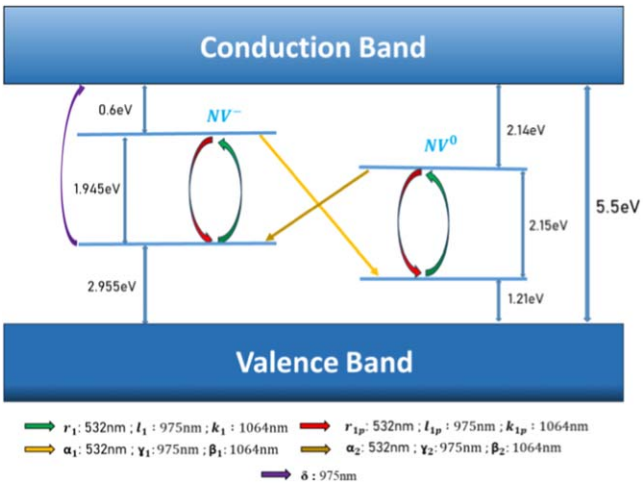

Figure 2. Energetically possible pathways for excitation, relaxation, ionization, and recombination processes between different energy levels [28, 33]. Green arrows indicate excitation processes associated with 532 nm(r_1), 975nm (l_1) and 1064nm (k_1). The red arrows represent relaxation processes governed by the excited state lifetimes, the yellow arrows describe ionization and recombination processes. δ is the two-photon ionization mechanism associated with 975 nm.

and the other half is passed to a spectrum analyzer (Research India, RI Series Spectrometer, Model No. RIFS-VSS-TEC). Diamond nanoparticles are trapped with two different IR sources emitting at 975 nm (Butterfly laser, Thorlabs) and 1064nm (diode laser, Lasever) and simultaneously illuminated with a green laser. The emission spectra of the diamond particles are recorded with the spectrum analyzer at different powers of the lasers. The two different IR sources are tuned to have similar powers at the sample stage. For each fixed power of IR laser, we measure the PL by varying the power of the green laser. To record data that is statistically significant as well as to boost signal-to-noise ratio, we performed measurements on nanodiamond clusters.

3. Modelling

We consider a four-level system as shown in figure 2 to simulate the NV charge dynamics under simultaneous green and IR illumination. The four-level system [32] is an effective model involving the ground and excited states of the two charge states of NVs (namely, NV^- and NV^0).

For a steady-state scenario, one has to solve the set of rate equations (in the matrix representation). Here I_g and I_{ir} in the evolution matrix correspond to the power of green and infrared (in this case, 975 nm) lasers respectively. The single-photon processes depend linearly on the laser power, whereas the two-photon processes are quadratic in nature. The ground state and the excited state are denoted by g_1, e_1 for NV^- and g_2, e_2 for NV^0. We treat the system as closed involving only four energy levels in total and impose the condition of conservation of NV population. We are performing continuous wave experiments at timescales which is substantially longer than the timescale of underlying physical processes occurring in the system. Consequently, the steady state condition is a reasonable assumption for the population change rate of energy levels.

$$\begin{bmatrix} -I_g r_1 - I_{ir}^2(l_1+\delta) & r_{1p} & 0 & I_g\alpha_2 + I_{ir}\gamma_2 & 0 \\ I_g r_1 + I_{ir}^2 l_1 & -I_g\alpha_1 - I_{ir}\gamma_1 - r_{1p} & 0 & 0 & 0 \\ I_{ir}^2\delta & I_g\alpha_1 + I_{ir}\gamma_1 & -I_g r_2 - I_{ir}^2 l_2 & r_{2p} & 0 \\ 0 & 0 & I_g r_2 + I_{ir}^2 l_2 & -I_g\alpha_2 - I_{ir}\gamma_2 - r_{2p} & 0 \\ 1 & 1 & 1 & 1 & -1 \end{bmatrix} \cdot \begin{bmatrix} g_1 \\ e_1 \\ g_2 \\ e_2 \\ 1 \end{bmatrix} = \begin{bmatrix} g_1 t \\ e_1 t \\ g_2 t \\ e_2 t \\ 0 \end{bmatrix} = \begin{bmatrix} 0 \\ 0 \\ 0 \\ 0 \\ 0 \end{bmatrix}$$

In the aforementioned evolution matrix, and figure 2, (r_1, r_{1p}), (l_1, l_{1p}), (k_1, k_{1p}) represent the excitation and relaxation rate of NV^- charge state under the illumination of wavelengths 532 nm, 975 nm, and 1064nm respectively; suffix 2 has been used to indicate the rates pertaining to NV^0 charge state. (α_1, γ_1, β_1), and (α_2, γ_2, β_2) denote the rates of ionization and recombination under the presence of wavelengths of 532 nm, 975 nm, and 1064 nm, respectively. The symbol δ corresponds to the charge state conversion process from NV^- to NV^0 by a two-photon mechanism under the illumination of 975 nm wavelength. For 1064nm illumination, $\delta = 0$ as the two-photon process leading to the ionization of NV^- from its ground state is energetically unfavorable.

We use experimental as well as reported data to fix as many parameters as possible to ensure that the final results remain reliable and unique. The excited-state lifetimes were taken to be 21 ns and 12 ns for NV^0 and

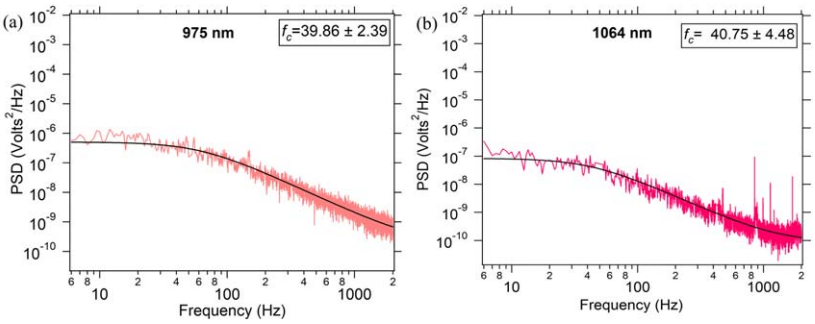

Figure 3. Power spectral density corresponding to the Brownian fluctuations of an NV bearing microdiamond of 0.5 μm diameter trapped in a 50 mW laser beam of (a) 975 nm and (b) 1064nm wavelength at the sample plane. The fitted curves according to equation (1) are shown in a solid black line.

Table 1. The table shows various parameters in the model with their effective values. The experimental data does not exhibit a nonlinear dependence on laser power, validating that all likely two-photon processes are irrelevant, at least, in the investigated illumination power density regime.

Parameters	Effective values
r_{1p}	$83.33\ \mu s^{-1}$
r_{2p}	$47.62\ \mu s^{-1}$
r_1, r_2	$16.70 \times 10^{-2}\ (\mu W)^{-1}$
α_1	$0.70 \times 10^{-2}\ \mu W^{-1}\mu s^{-1}$
α_2	$1.51 \times 10^{-2}\ \mu W^{-1}\mu s^{-1}$
β_1	$0.28 \times 10^{-2}\ \mu W^{-1}\mu s^{-1}$
β_2	$0.45 \times 10^{-2}\ \mu W^{-1}\mu s^{-1}$
γ_1	$0.05 \times 10^{-2}\ \mu W^{-1}\mu s^{-1}$
γ_2	$0.08 \times 10^{-2}\ \mu W^{-1}\mu s^{-1}$
l_1, l_2, k_1, k_2	$0.00\ (\mu W)^{-2}$
$k_{1p}, k_{2p} l_{1p}, l_{2p}$	$0.00\ \mu s^{-1}$
δ	$0.00\ \mu W^{-2}\mu s^{-1}$

NV^-, respectively [34]. The ionization rate for 532 nm illumination is chosen to match those reported by Aslam *et al* [32]; in both of these studies, the optical setups and, consequently, the laser power densities at the sample plane are reasonably analogous. The recombination rate for our specific system is the only free parameter under green excitation, which can be readily evaluated by taking into account the PL ratios associated with the two states, i.e. $\frac{PL_{NV^-}}{PL_{NV^0}}$. This ratio was obtained experimentally from integrated, background-corrected PL by splitting it into two parts, below (related to NV^0) and above (related to NV^-) 650 nm, and was taken as input to our model (figure 5(c)). Moreover, the data does not show any non-linear behavior as a function of IR laser powers; thus, the simulation ignores the virtual two-photon process (δ, l_1, l_2, etc.). The extracted values of the effective parameters are listed in table 1.

4. Results and discussions

We optically trap a single microdiamond particle in water with two different IR lasers at 50 mW power. The power spectral densities(PSD) for positional fluctuations of a nanodiamond in an optical trap are shown in figures 3(a) and (b). The experimentally obtained (PSD) are fitted to the general form for PSD of an optically trapped particle in a pure viscous medium given by equation (1) [35, 36]. The corner frequency f_c is related to the trap stiffness κ as $f_c = \frac{\kappa}{\gamma}$ where γ is the drag coefficient experienced by a spherical particle in the viscous medium. Since PSD data is recorded as voltage fluctuations in the photodiode, a conversion factor $'\beta'$ is multiplied to convert it from V^2/Hz to nm^2/Hz.

$$PSD = \beta^2 \frac{\frac{k_B T}{\gamma}}{4\pi^2 (f^2 + f_c^2)}. \quad (1)$$

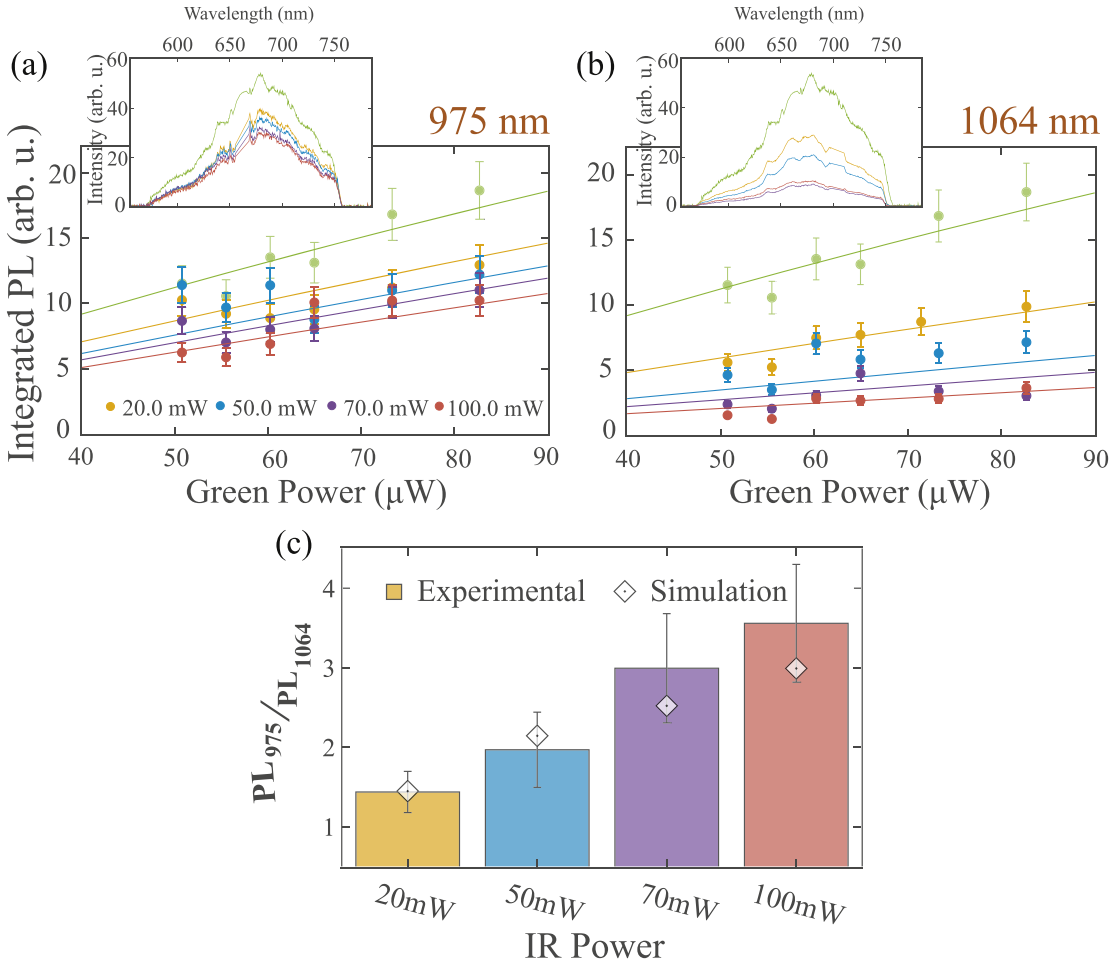

Figure 4. Integrated PL (area under the PL curve) plotted against the excitation laser(green) power with simultaneous (a) 975 nm illumination and (b) 1064 nm illumination shows a decreasing trend with increase in power of IR from 20 mW to 100 mW. The wavelength dependent PL curves at the corresponding powers of 975 nm and 1064nm are shown as insets of (a) and (b) The green curve represents the reference PL spectrum under green illumination. PL emission in the absence of IR wavelengths is shown in green in both (a) and (b), and their corresponding insets. The markers in plots (a) and (b) represent the experimental data, while the error-bars result from the time-dependent PL fluctuations (~10%) occurring during the data collection interval. (c) Ratios of integrated PL intensities at different powers of 975 nm and 1064nm averaged across different powers of the exciting wavelength (green laser). Subsequently, the lines in (a) and (b) and markers in (c) depict the simulation results.

From the results shown in figure 3, we find the trap stiffness to be $1.93 \pm 0.11\ pN\mu m^{-1}$ and $1.88 \pm 0.06\ pN\mu m^{-1}$ when microdiamonds of diameter 0.5 μm are trapped with beams of 1064 and 975 nm, respectively. Similar trap stiffness values indicate that trapping is not affected by changing the wavelength of the trapping laser. These results signify that the wavelengths do not alter the trapping characteristics; however, NV PL is considerably modified.

We examine the PL of a diamond excited with a 532 nm (green) laser under different powers of IR illumination. The PL spectra are recorded in the range of 550 nm to 800 nm to include emissions from both NV^0 and NV^- centers as shown in the insets of figure 4. It is difficult to retain the same cluster in the optical trap throughout the long experimental duration. This is because the high refractive index of nanodiamonds makes it conducive for the particle to be removed from the trap. In addition, as the diamonds used in the experiment contain many NV centers, adding more particles simply increases the PL collection intensities. Therefore, for each selected cluster, we collect the PL spectrum under only green laser illumination, and the scaling factor is obtained by taking the ratio of this signal with the reference PL spectrum under green illumination (see green spectrum presented in the inset of figure 4). The same scaling factor is used to rescale all the other PL spectra under simultaneous green laser and IR laser illuminations. We obtain the integrated PL for figures 4(a) and (b) by integrating the photoluminescence intensity over the wavelength range. Additionally, by splitting integrated PL into two sections, below and above 650 nm, we experimentally determine the PL ratio of the two charge states, NV^0 and NV^-, respectively. The PL spectrum obtained by illuminating the green laser is plotted in the insets of figure 4.

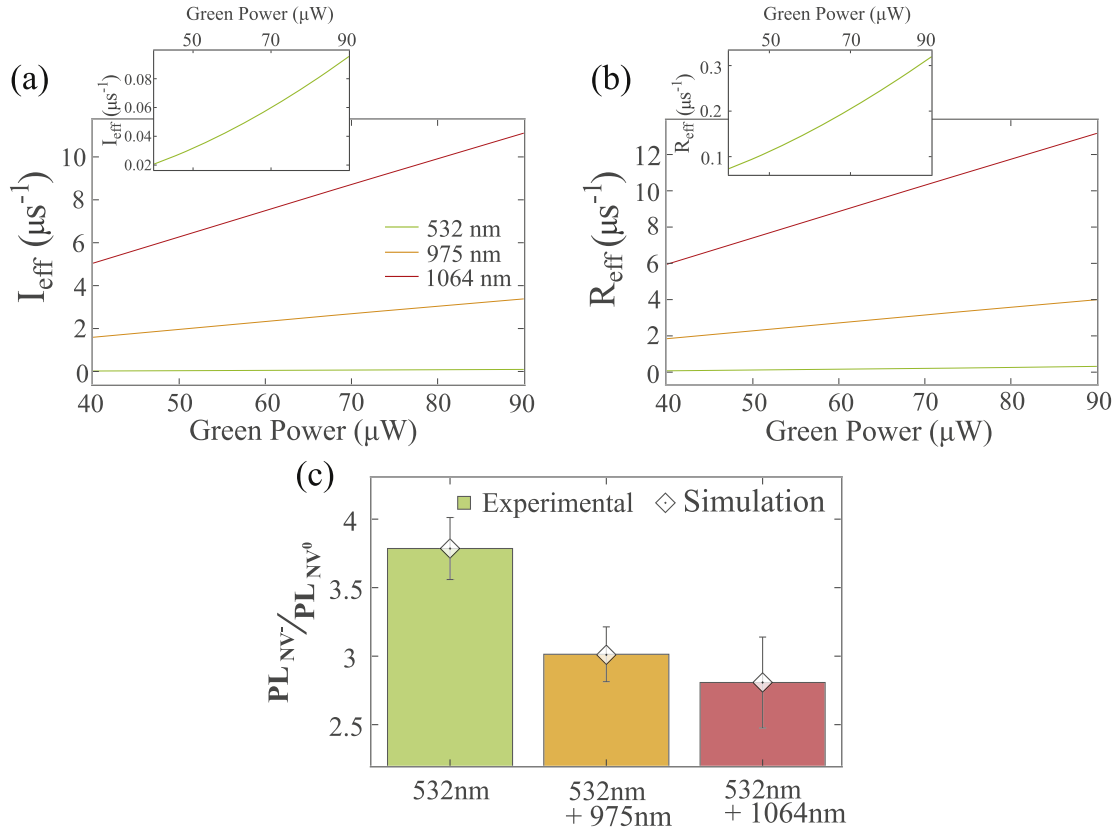

Figure 5. Charge state conversion rates extracted from the model at the maximum power (100 mW) of IR wavelengths - (a) effective ionization rate [$I_{eff} = (\alpha_1 I_g + \gamma_1 I_{ir,975} + \beta_1 I_{ir,1064}) \cdot \frac{e_1}{e_1+g_1}$], and (b) effective recombination rate $\left[R_{eff} = (\alpha_2 I_g + \gamma_2 I_{ir,975} + \beta_2 I_{ir,1064}) \cdot \frac{e_2}{e_2+g_2} \right]$. There is a rise in both I_{eff} and R_{eff}, the change being greater for 1064nm than 975 nm. The insets show close to quadratic dependence of ionization and recombination rates on green laser power as expected for two photon processes, (c) comparison between mean PL ratios $(\frac{PL_{NV^-}}{PL_{NV^0}})$ obtained from the experiments and the simulations for varied excitation conditions. In the simulation for solely 532 nm illumination, we use $PL_{NV^-} = r_{1p} e_1$ and $PL_{NV^0} = r_{2p} e_2$, extra terms with the appropriate coefficients are added in the expression with the introduction of infrared wavelengths.

The primary observation is that the quenching of PL is more pronounced for 1064nm excitation as compared to 975 nm excitation. Particularly, at the highest achievable green power (~83 μW) and IR power (~100 mW) in our setup, we see an approximate 45% reduction in intensity for 975 nm illumination, whereas, for 1064 nm illumination, PL intensity reduces by 80%. Additionally, the reduction of PL intensity depends on the applied power of IR laser illumination. This is summed up in figure 4(c) as ratios of PL intensities under excitation with the two IR wavelengths averaged over the powers of green laser.

At first glance, it appears that one can match the observations just by obtaining an appropriate PL ratio of the two charge states for the used IR laser illuminations. This is because the excited state lifetimes of NV^- and NV^0 are different and they can indeed affect the overall PL intensity. However, these PL ratios (as shown in figure 5(c)) by themselves are insufficient to explain the degree of quenching observed in the experimental data. Essentially, the drop in intensity across the whole PL spectrum requires mechanisms that can remove the electron from the excited state of both of the charge states before they can relax to the ground state by emitting a photon. The experimental data can only be explained if we take into account the dependence of ionization and recombination rates on IR wavelengths. The simulations ascertain that under 1064nm excitation both the rates must be higher than those obtained in the case of 975 nm excitation as shown in figures 5(a) and (b). This inference also suggests that 975 nm laser excitation is not only suitable to obtain higher count-rates but also to preserve NV charge and spin states for longer duration. Simple energy arguments are inadequate to justify the effectiveness of 1064nm laser at inducing rapid cycling of NV charge states, and further investigations are required to understand the origin of the wavelength-dependent ionization and recombination cross-sections.

The implemented theoretical model is certainly rudimentary and does not involve any mechanism that has not already been firmly established. Nonetheless, it can definitely be thought of as an effective model with effective coefficients of the complex system involving multiple-charge states and other defect states such as nitrogen [37] and surface states [38]. Thus, our speculations imply that some unidentified processes are playing a major role in determining the charge (and possibly spin) dynamics at the investigated IR wavelengths. Other

speculations to account for PL quenching include hard-to-probe mechanisms like multiphoton absorption processes [29], Jahn-Teller like splitting of energy levels due to interaction of the lattice with IR photon [28], and spin dependent charge state interconversion [29, 31]. However, our data can not prove or disprove any of these mechanisms. Additionally, our model proposes a possibility of wavelength-dependent dynamics among various charge states of NVs, which has not been presented in the reported literature. It is currently unclear whether this phenomenon is only present in nanodiamonds and in samples containing high-density NV ensembles, thus, systematic wavelength-dependent PL analysis of samples having varied defect concentrations is necessary to shed more light on the underlying physics.

Diamond with NVs is a standard material used for approaching quantum sensing. The NV centers can be addressed with a 532 nm laser, while the diamond particle itself can be simultaneously confined within an optical trap. It is known in the community that 1064nm, which is a standard wavelength for optical trapping, especially in biological systems, affects the PL intensity when used in conjugation with 532 nm laser. We report here that another standard wavelength, 975 nm, is a much better choice for optical trapping.

5. Conclusion

In summary, we find that the PL emission from NV nanodiamonds is significantly higher for 975 nm illumination as compared to that for 1064nm illumination while the optical trap stiffness is comparable for both the infrared wavelengths. Our simulations suggest, amongst two studied wavelengths, illumination of 1064 nm laser results in fast charge-state transformations. While the cause of this effect is currently unknown, our observations establish that a laser of 975 nm wavelength is more suitable for trapping nanodiamonds when its PL is conjointly utilized.

Acknowledgments

The authors thank the Indian Institute of Technology, Madras, India, for its seed and initiation grants to B.R. and S.D. S.D. and A.G. acknowledge the use of facilities supported by a grant from the Mphasis F1 Foundation given to the Centre for Quantum Information, Communication, and Computing (CQuICC). S.D. also thanks Science and Engineering Research Board (SERB Grant No. SRG/2023/000322), India for start-up funding. This work was also supported by the DBT/Wellcome Trust India Alliance Fellowship IA/I/20/1/504900 awarded to Basudev Roy.

Data availability statement

The data cannot be made publicly available upon publication because no suitable repository exists for hosting data in this field of study. The data that support the findings of this study are available upon reasonable request from the authors.

Disclosures

The authors declare no conflicts of interest.

ORCID iDs

Siddharth Dhomkar https://orcid.org/0000-0002-0843-3826
Basudev Roy https://orcid.org/0000-0003-0737-2889

References

[1] DiVincenzo D P 2000 The physical implementation of quantum computation *Fortschritte der Physik: Progress of Physics* **48** 771–83
[2] Schirhagl R, Chang K, Loretz M and Degen C L 2014 Nitrogen-vacancy centers in diamond: Nanoscale sensors for physics and biology *Annu. Rev. Phys. Chem.* **65** 83–105
[3] Neumann P, Beck J, Steiner M, Rempp F, Fedder H, Hemmer P R, Wrachtrup J and Jelezko F 2010 Single-shot readout of a single nuclear spin *Science* **329** 542–4
[4] McGuinness L P *et al* 2011 Quantum measurement and orientation tracking of fluorescent nanodiamonds inside living cells *Nat. Nanotechnol.* **6** 358–63
[5] Doherty M W, Manson N B, Delaney P, Jelezko F, Wrachtrup J and Hollenberg L C 2013 The nitrogen-vacancy colour centre in diamond *Phys. Rep.* **528** 1–45

[6] Lokesh M, Nalupurackal G, Roy S, Chakraborty S, Goswami J, Gunaseelan M, Chowdhury I U, Bhallamudi V P, Mahapatra P S and Roy B 2023 Accelerated self assembly of particles at the air-water interface with optically assisted heating due to an upconverting particle *Opt. Express* **31** 5075–86
[7] Balasubramanian G *et al* 2008 Nanoscale imaging magnetometry with diamond spins under ambient conditions *Nature* **455** 648–51
[8] Maze J R *et al* 2008 Nanoscale magnetic sensing with an individual electronic spin in diamond *Nature* **455** 644–7
[9] Mamin H, Kim M, Sherwood M, Rettner C, Ohno K, Awschalom D and Rugar D 2013 Nanoscale nuclear magnetic resonance with a nitrogen-vacancy spin sensor *Science* **339** 557–60
[10] Staudacher T, Shi F, Pezzagna S, Meijer J, Du J, Meriles C A, Reinhard F and Wrachtrup J 2013 Nuclear magnetic resonance spectroscopy on a (5-nanometer) 3 sample volume *Science* **339** 561–3
[11] Häberle T, Schmid-Lorch D, Reinhard F and Wrachtrup J 2015 Nanoscale nuclear magnetic imaging with chemical contrast *Nat. Nanotechnol.* **10** 125–8
[12] Hapuarachchi H, Campaioli F and Cole J H 2022 Nv-plasmonics: modifying optical emission of an nv- center via plasmonic metal nanoparticles *Nanophotonics* **11** 4919–27
[13] Kumar S, Lausen J L, Garcia-Ortiz C E, Andersen S K, Roberts A S, Radko I P, Smith C L, Kristensen A and Bozhevolnyi S I 2015 Excitation of surface plasmon polariton modes with multiple nitrogen vacancy centers in single nanodiamonds *J. Opt.* **18** 024002
[14] Schrand A M, Huang H, Carlson C, Schlager J J, Ōsawa E, Hussain S M and Dai L 2007 Are diamond nanoparticles cytotoxic? *The Journal of Physical Chemistry* B **111** 2–7
[15] Chao J-I, Perevedentseva E, Chung P-H, Liu K-K, Cheng C-Y, Chang C-C and Cheng C-L 2007 Nanometer-sized diamond particle as a probe for biolabeling *Biophys. J.* **93** 2199–208
[16] Krüger A, Liang Y, Jarre G and Stegk J 2006 Surface functionalisation of detonation diamond suitable for biological applications *J. Mater. Chem.* **16** 2322–8
[17] Lovchinsky I *et al* 2016 Nuclear magnetic resonance detection and spectroscopy of single proteins using quantum logic *Science* **351** 836–41
[18] Zhang T *et al* 2021 Toward quantitative bio-sensing with nitrogen-vacancy center in diamond *ACS Sensors* **6** 2077–107
[19] Miller B S *et al* 2020 Spin-enhanced nanodiamond biosensing for ultrasensitive diagnostics *Nature* **587** 588–93
[20] Aslam N, Zhou H, Urbach E K, Turner M J, Walsworth R L, Lukin M D and Park H 2023 Quantum sensors for biomedical applications *Nature Reviews Physics* **5** 157–69
[21] Ajoy A *et al* 2018 Orientation-independent room temperature optical ^{13}c hyperpolarization in powdered diamond *Science Advances* **4** eaar5492
[22] Tegafaw T, Liu S, Ahmad M Y, Ali Al Saidi A K, Zhao D, Liu Y, Yue H, Nam S-W, Chang Y and Lee G H 2023 Production, surface modification, physicochemical properties, biocompatibility, and bioimaging applications of nanodiamonds *RSC Adv.* **13** 32381–97
[23] Geiselmann M, Marty R, Abajo F J G D and Quidant R 2013 Fast optical modulation of the fluorescence from a single nitrogen-vacancy centre *Nat. Phys.* **9** 785–9
[24] Horowitz V R, Alemán B J, Christle D J, Cleland A N and Awschalom D D 2012 Electron spin resonance of nitrogen-vacancy centers in optically trapped nanodiamonds *Proc. Natl Acad. Sci.* **109** 13493–7
[25] Russell L W, Ralph S G, Wittick K, Tetienne J-P, Simpson D A and Reece P J 2018 Manipulating the quantum coherence of optically trapped nanodiamonds *ACS Photonics* **5** 4491–6
[26] Lokesh M, Vaippully R, Nalupurackal G, Roy S, Bhallamudi V P, Prabhakar A and Roy B 2021 Estimation of rolling work of adhesion at the nanoscale with soft probing using optical tweezers *RSC Adv.* **11** 34636–42
[27] Lai N D, Faklaris O, Zheng D, Jacques V, Chang H C, Roch J F and Treussart F 2013 Quenching nitrogen-vacancy center photoluminescence with an infrared pulsed laser *New J. Phys.* **15** 033030
[28] Ji P and Dutt M V 2016 Charge state dynamics of the nitrogen vacancy center in diamond under 1064-nm laser excitation *Phys. Rev.* B **94** 024101
[29] Hopper D A, Grote R R, Exarhos A L and Bassett L C 2016 Near-infrared-assisted charge control and spin readout of the nitrogen-vacancy center in diamond *Phys. Rev.* B **94** 241201
[30] Meirzada I, Hovav Y, Wolf S A and Bar-Gill N 2018 Negative charge enhancement of near-surface nitrogen vacancy centers by multicolor excitation *Phys. Rev.* B **98** 245411
[31] Roberts R P, Juan M L and Molina-Terriza G 2019 Spin-dependent charge state interconversion of nitrogen vacancy centers in nanodiamonds *Phys. Rev.* B **99** 174307
[32] Aslam N, Waldherr G, Neumann P, Jelezko F and Wrachtrup J 2013 Photo-induced ionization dynamics of the nitrogen vacancy defect in diamond investigated by single-shot charge state detection *New J. Phys.* **15** 013064
[33] Subedi S, Fedorov V, Peppers J, Martyshkin D, Mirov S, Shao L and Loncar M 2019 Laser spectroscopic characterization of negatively charged nitrogen-vacancy (nv -) centers in diamond *Opt. Mater. Express* **9** 2076
[34] Storteboom J, Dolan P, Castelletto S, Li X and Gu M 2015 Lifetime investigation of single nitrogen vacancy centres in nanodiamonds *Opt. Express* **23** 11327
[35] Berg-Sørensen K and Flyvbjerg H 2004 Power spectrum analysis for optical tweezers *Rev. Sci. Instrum.* **75** 594–612
[36] Pesce G, Jones P H, Maragò O M and Volpe G 2020 Optical tweezers: theory and practice *The European Physical Journal Plus* **135** 1–38
[37] Jayakumar H, Henshaw J, Dhomkar S, Pagliero D, Laraoui A, Manson N B, Albu R, Doherty M W and Meriles C A 2016 Optical patterning of trapped charge in nitrogen-doped diamond *Nat. Commun.* **7** 12660
[38] Dhomkar S, Jayakumar H, Zangara P R and Meriles C A 2018 Charge dynamics in near-surface, variable-density ensembles of nitrogen-vacancy centers in diamond *Nano Lett.* **18** 4046–52